Wear Test Demonstration of a Technique to Mitigate Keeper Erosion in a High-Current LaB_6 Hollow Cathode

Amanda K. Ho,* Benjamin A. Jorns,† Ioannis G. Mikellides,‡ Dan M. Goebel,§ and Alejandro Lopez Ortega¶
Jet Propulsion Laboratory, California Institute of Technology, Pasadena, CA 91109, USA

The results of a wear test on a 100-A LaB_6 hollow cathode are presented as verification of a technique to mitigate keeper erosion caused by sputtering from anomalously high-energy ions. The ions responsible for this erosion have been theorized to result from the onset ion acoustic turbulence in the plume of the cathode. The proposed technique to minimize the erosion relies on identifying operating conditions where the energy of the ion acoustic turbulence is low. 100 hour wear tests are conducted on a high-current hollow cathode with a molybdenum keeper at three operating conditions: two with low turbulence levels and one with high turbulence levels. It is demonstrated that the keeper exhibits low levels erosion (at a peak erosion rate of around 0.035 um/hour) that can be explained by classical mechanisms at the low turbulence states, and anomalously high sputtering (at a peak erosion rate of .07 um/hour) at the high erosion state.

*Engineer, Spacecraft Design Group, 4800 Oak Grove Dr., MS T1722-, Pasadena, CA, 91109, amanda.k.ho@jpl.nasa.gov
†Engineer, Electric Propulsion Group, 4800 Oak Grove Dr., MS 125-109, Pasadena, CA, 91109, benjamin.a.jorns@jpl.nasa.gov
‡Principal Engineer, Electric Propulsion Group, 4800 Oak Grove Dr., MS 125-109, Pasadena, CA, 91109, Ioannis.G.Mikellides@jpl.nasa.gov
§Senior Research Scientist, Thermal and Propulsion Engineering Section, 4800 Oak Grove Dr., MS 125-109, Pasadena, CA, 91109, Dan.M.Goebel@jpl.nasa.gov
¶Engineer, Electric Propulsion Group, 4800 Oak Grove Dr., MS 125-109, Pasadena, CA, 91109, Alejandro.Lopez.Ortega@jpl.nasa.gov

©2016 California Institute of Technology. Government sponsorship acknowledged.

Nomenclature

a_L	= Lindhard screening length, Å
E	= ion energy, eV
E_{th}	= threshold energy and fit parameter, eV
$f(E)$	= ion energy distribution function
m_i	= mass of xenon ion, kg
M_1	= mass of projectile particle (xenon ion), amu
M_2	= mass of target particle (molybdenum), amu
n_i	= ion density, m^{-3}
s_n^{KrC}	= Kr-C potential nuclear stopping cross section
s_n^{TF}	= Thomas-Fermi nuclear stopping cross section
q	= elementary charge, C
Z_1	= atomic number of projectile particle (xenon ion)
Z_2	= atomic number of target particle (molybdenum)
α	= energy-independent function
β	= fit parameter
ϵ	= reduced energy
ε_T	= erosion rate, um $hour^{-1}$
η	= fit parameter
γ	= sputter yield, atoms ion^{-1}
ϕ_i	= ion flux, ion m^{-2} s^{-1}

I. Introduction

The increasing scope and scale of the next-generation of proposed deep-space NASA missions, such as the Asteroid Redirect Mission, has led to a pressing need to develop higher-power electric propulsion systems with longer life. On the proposed timescales for these missions (> 2 years), however, a number of erosion processes can lead to failure modes.[18,19] The erosion of the hollow cathode keeper is one of the most problematic of these modes—particularly when operated at high currents. Indeed, in the only long-term wear test do date on a high-current cathode (100 A), Brophy and Garner[17] showed cathode failure after only 1000 hours. This is just a small fraction of the required life for multi-year, deep space missions.

The erosion of the hollow cathode keeper at high discharge currents is the result of sputtering from anomalous energetic ions.[3, 17, 20-24] These ions are termed anomalous because classical processes such as electrostatic acceleration due to potential gradients and pressure-driven acceleration do not provide sufficient energy to explain their presence in the cathode plume. While a number of studies have examined the potential source for these ions,[23, 25-29] a recent two-year internal research campaign at the NASA Jet Propulsion Laboratory on a 100-A LaB_6 cathode established that at high discharge currents, there is a correlational and causal link between the formation of high-energy ions and the onset of ion acoustic turbulence in the plume.[1,2,6] This previous work showed how ion acoustic turbulence is driven unstable in hollow cathode plumes due to the large relative electron drift with respect to ions and that the onset of this turbulence causes high anomalous electron resistivity in the plume.[30] The growth of this turbulence in turn is balanced by ion Landau damping which leads the formation of an energetic ion tail in the plume.[1] A recent experimental work[31] has explicitly showed the formation of this tail through Laser Induced Fluoresce measurements of the ion velocity distribution function in the plume.

The results of these fundamental investigation into IAT in the cathode plume guided a subsequent parametric analytical and experimental study wherein the correlation between ion energy in the plume and turbulence was verified over a wide range of operating conditions. This investigation also showed that through a judicious choice of operating conditions, high-current operation with low turbulence levels can be achieved. This suggested a potential technique for mitigating the energetic ions and their associated erosion at high currents: optimizing the cathode operation/design to prevent or minimize the onset of IAT.

One of the major limitations from this previous study on mitigation, however, was that the ion energy measurements were performed downstream of the keeper. Thus, even though it was apparent from both kinetic models[30] and experimental results[6] that minimizing the IAT reduced energetic ions downstream of the cathode, there was an open question as to whether or not eliminating the IAT would reduce energetic ions (and therefore erosion) at the keeper face. The purpose of this work is to address this question by performing 100 hr wear tests to measure directly the erosion on the face of the cathode keeper at conditions where low and high levels of turbulence have been observed. With this purpose in mind, this paper is organized in the following way. In the first section, we describe the experimental setup and data analysis techniques. In the second, we and use the results of previous studies on IAT to guide the choice of operating conditions for the wear tests. In the third section, we present the experimental results. And in the fourth and final section, we discuss our results in the context of erosion predictions and the implications for this mitigation technique.

II. Experimental Setup

A. **Cathode Assembly/Vacuum Chamber**

The cathode assembly for the wear tests consists of a graphite tube housing a LaB_6 insert. The cathode tube is wrapped in a tantalum coaxial heater, housed inside of a molybdenum cathode keeper. The keeper orifice to keeper diameter ratio is 30%. There is a tungsten endplate at the end of the cathode tube that is 12% the diameter of cathode tube orifice. The setup (Fig. 1) is installed in the JPL High Current Test Facility, a 2.8 m x 1.3 m cylindrical chamber with vacuum maintained by two cryopumps. The base pressure of this facility is $\sim 10^{-8}$ Torr . At the flow rate of 10 sccm xenon, the background pressure is maintained at $1.0 \times 10{-}4$ Torr, and at a flow rate of 15 sccm, the background pressure is maintained at $2.0 \times 10{-}4$ Torr. The anode is a water-cooled, copper cylinder lined with tungsten. The cathode assembly is placed in the vacuum chamber so that the keeper face is 3 cm upstream from the start of the anode cylinder.

We chose to use a molybdenum keeper for this study because of its resistance to deformation at the high emitter temperatures during cathode operation. Previous investigations referenced here were performed with a graphite keeper, but a parametric study we performed revealed that the plasma properties, i.e. oscillations and ion energy, remained unchanged by this change in keeper material.

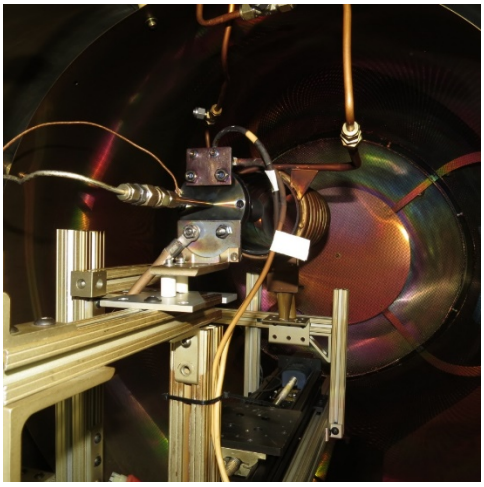

Figure 1. Cathode setup installed in the vacuum chamber facility.

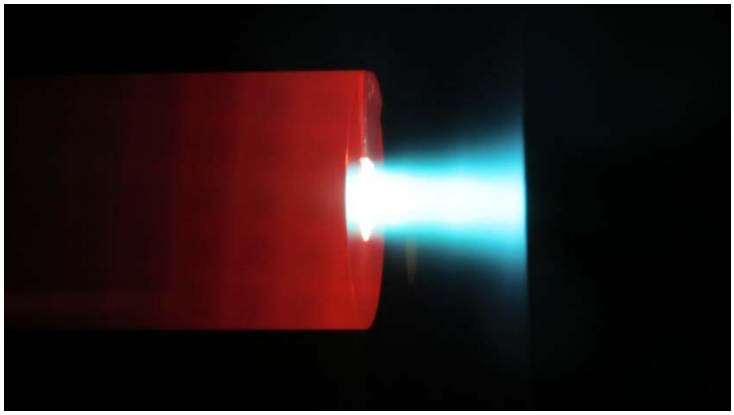

Figure 2. Cathode running at the first operating condition.

In order to keep a reference area protected from ion sputtering, a molybdenum shield was spot welded on the surface of the keeper with silver nickel strip in between the two molybdenum surfaces. The shield covers 30 degrees of the surface of the molybdenum keeper.

Figure 3. Cathode keeper with molybdenum shield spot-welded on, prior to start of campaign.

B. Experimental Procedure

We performed wear tests at three operating conditions on this 100-A cathode (see Sec. III) For each condition, the cathode ran for 25 hour intervals in the vacuum chamber, for up to 125 hours. As a note, because circumstances rendered the first 25 hour intervals for each case ambiguous either because of stress relieving or operator error, the initial case for each condition became the face of the keeper after the first 25 hours. Prior to each 25-hour trial, the molybdenum shield was spot welded onto the surface of the cathode keeper. After each trial, the shield was carefully peeled off, and the topography of the keeper face was measured using a Nanovea ST400 Confocal Chromatic Profilometer. The optic pen used for the scans was the CL2/MG210 300 um Optical Pen.

The cathode keeper face is scanned as a Cartesian scan of the surface, in which the scanning axis incremented in the X direction and the index axis incremented in the Y direction. The scanning resolution is 9 um and the index axis resolution is 30 um. The max accepted linearity error rated for the sensor is 3 um. We found in practice that the average noise on a measurement was +/-5um, and that the standard deviation of a measurement was 1.13 um.

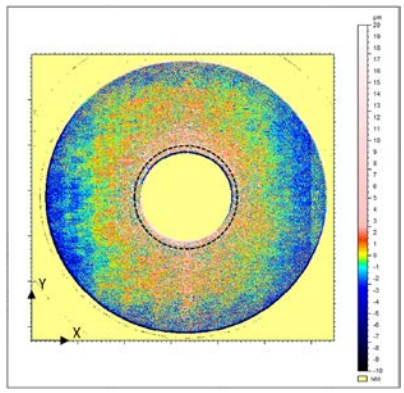

Figure 4. Scan of the initial cathode keeper face using the Nanovea ST400 profilometer. Scan generated with the Nanovea Expert 3D Analysis Software.

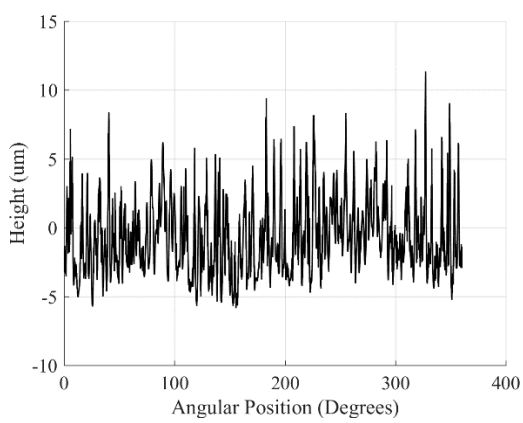

Figure 5. Raw data of a concentric profile centered about the cathode center, at a distance 4% of the keeper radius. Approximate location indicated on Fig. 4.

C. Experimental Procedure

We show in Fig. 4 a representative scan for the keeper face that was taken before the wear testing. The profilometer scans were first leveled using the Nanovea Expert 3D Analysis software. The leveling operation in the program took user-specified points on the raw scan of the keeper to fit a plane, and then subtracted the local height difference between points of the fitted plane to a leveled plane. The scan then was imported into Matlab. The concentric

profiles (centered about the cathode keeper center) of the Cartesian scan were extracted for each 25 hour trial. Each concentric profile plot at a particular radial location was the average of the radial surface across a range of 0.05 cm. These concentric plots were then imposed on top of those from the initial hour case, with the shielded regions used as a zero reference. Fig. 5 illustrates an example concentric plot after 125 hours, plotted on the concentric plot at the same radial location after 25 hours.

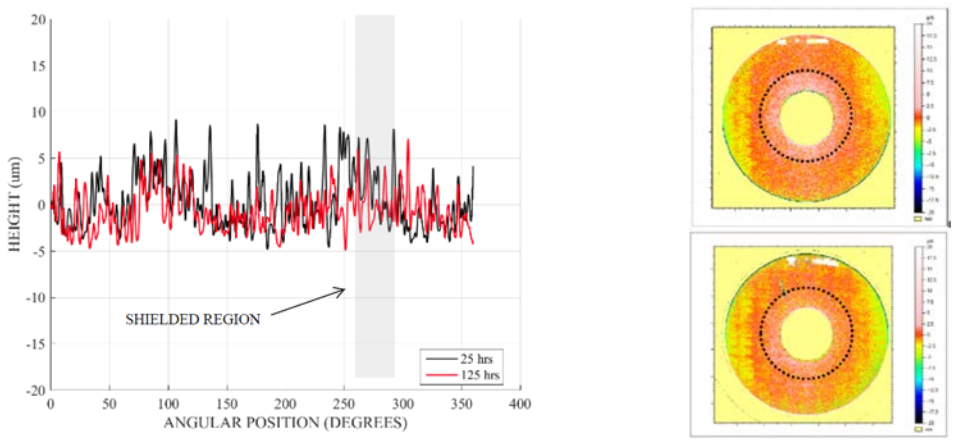

(a) (b)

Figure 6. (a.) Example plots of concentric profiles from 25 hour keeper face and 125 hour keeper face at the low current wear condition (See Sec. III) imposed on top of each other at the same radial location. Shielded region indicated in grey. (b.) Profilometer scans of 25 hour keeper face and 125 hour keeper face, dotted line shown is approximate concentric profile extracted in (a).

The overall average erosion for each operating case is then found as an average of the unshielded keeper face regions of the initial trial subtracted by the unshielded keeper face regions of the final trial, as a function of radial distance from the center of the cathode keeper.

III. Wear Test Operating Conditions

We show in Fig. 7 the results of a parametric investigation from Ref. 2 to measure the IAT energy in the plume of the same 100-A hollow cathode described in Sec. II . This figure demonstrates that for a fixed flow rate of xenon, there is a characteristic inflection point with discharge current where the turbulent energy is minimized. The reason for this inflection point is due to the different dependencies on discharge current of the steady-state driving term (electron drift) and damping term (ion-neutral collisions) for the IAT in the plume. This same study showed that the trends in turbulence energy are mirrored by the trends in ion energy downstream of the cathode (Fig. 7b). This figure shows the standard deviation in ion energy as measured with a retarding potential analyzer placed downstream and off-axis from the cathode. Larger energy spread in this case corresponds to the presence of higher energy ions.

The results in Fig. 7 suggest a mitigation strategy for erosion. In particular, if we require a fixed flow rate from the keeper operating at high current, then in order to minimize the turbulent energy, we can tune the discharge current until the minimum at the inflection point is achieved. Similarly, if we require a fixed discharge current, we can increase the flow rate until the turbulence is damped and the ion tail is eliminated. It should be noted here that the reduction in energetic ions with increasing flow rate likely cannot be attributed to the collision of these particles with an increased neutral background. This is because the cross-section for these collisions exceeds the dimensions of the experimental setup by a factor of 2-4 for all of the flow rates shown here.

As mentioned in Sec. 1, while it is evident that these mitigation techniques translate to reduction of the energetic ions and turbulence downstream of the keeper, it is still not known if the sputtering of the keeper similarly will be reduced. In order to address this question, we select three operating conditions for wear testing in line with the mitigation strategy outlined above. These are shown high-lighted in Fig. 7b. First, we operate at a seemingly high-erosion (HE1) condition, 140 A and 10 sccm where both high turbulence and high energy ions in the plume are observed. Second, assuming constant flow is the requirement, we invoke the first mitigation technique (M1) by moving to the condition 75 A and 10 sccm located at the minimum of the curve in Figs. 7a and b. Third, we make constant high current the requirement and invoke the second mitigation technique (M2)---operating at 140 A but at higher flow rate, 15 sccm.

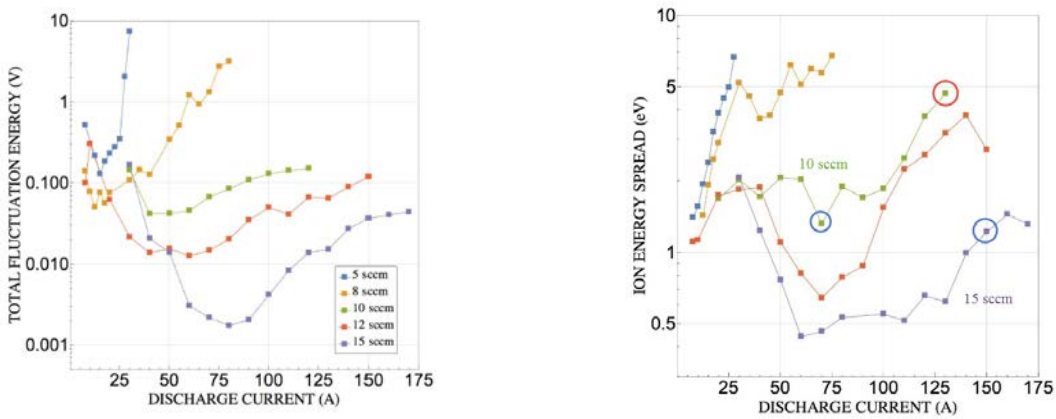

(a) (b)

Figure 7 (From Ref.2). a) Wave energy as a function of discharge current for different flow rates b) Ion energy spread for the same operating conditions

If it is in fact the case that the ion energy content is the same at the keeper as measured downstream (Fig. 8), we can show that the high erosion case, HE, and two mitigation techniques, M1 and M2, should directly translate to reduced erosion at the keeper. In particular, by invoking previous measurements[2] including the downstream ion energy, we can calculate the erosion rate given along the surface of the keeper in units of um/hour by

$$\varepsilon_T = 3.6 \times 10^9 \int_0^\infty \gamma(E)\, \phi_i(E) dE \tag{1}$$

where gamma denotes the sputtering yield as a function of ion energy, E, (Appendix) and the ion flux density distribution is

$$\phi_i(E) = n_i \left(\frac{2q}{m_i} (E - V_p) \right)^{1/2} f(E) dE \tag{2}$$

Here n_i is plasma density at location, m_i is mass of ion, q is elementary charge, $f(E)$ is energy distribution function of ions, and V_p is the plasma potential, which we take as the discharge voltage.

For the density in Eq. 1, we note that In Ref. 2, this parameter was measured for the high erosion case (140 A and 10 sccm), as a function of radius from the cathode centerline, as shown in Fig. 9 These measurements were taken in one radial direction (3 cm downstream of the cathode) from a location near the centerline, and then mirrored across the other radial direction. We do not have spatially resolved measurements for the other wear conditions. However, as seen from measurements taken at centerline from Ref. 2 (Fig. 8), the plasma density does not generally

vary significantly between different flow rates, holding discharge current constant. As such, the plasma density for the low erosion, higher current case (140 A and 15 sccm) is assumed to have the same profile as that of the high erosion case (see Fig. 9). Because the plasma density is relatively flat at the surface of the keeper, we take the averaged plasma density at that location. The plasma density profile is scaled down, using the ratio between the peak plasma density data points at centerline near the keeper (Fig. 8) for each current case. For the ion energy, the ion energy distributions that were measured 10 centimeters off cathode axis and downstream of the keeper (Fig. 10)---making the previously mentioned assumption that the energetic content at the keeper is the same. We also make the assumption that the ions are normally incident on the keeper.

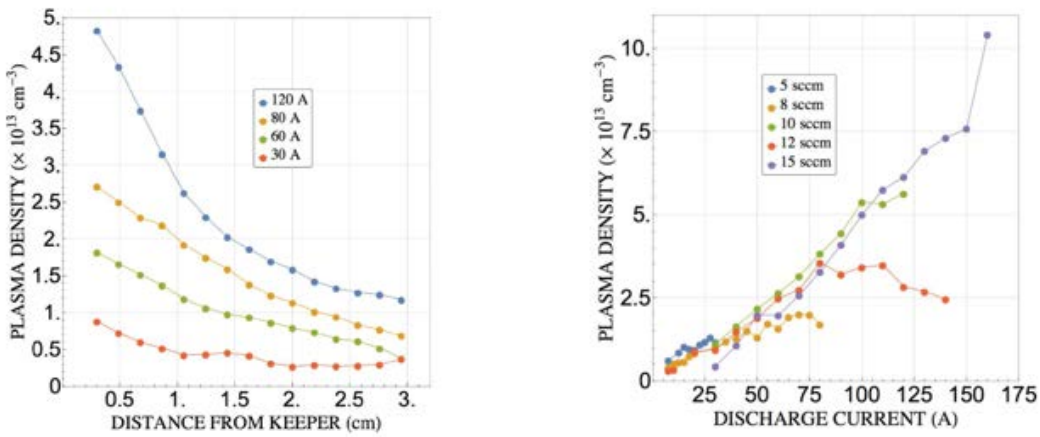

(a) (b)

Figure 8 (From Ref. 2). a) Plasma density as a function of distance from keeper face on cathode line, for a flow rate of 15 sccm. b) Spatially averaged plasma density as a function of discharge current for five flow rates.

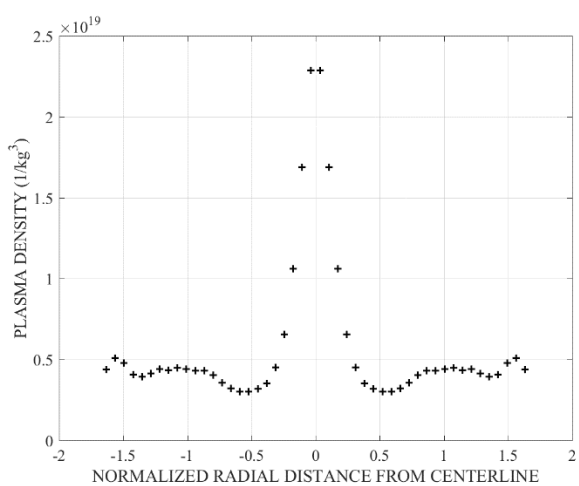

Figure 9. Plasma density data points for the 140 A and 10 sccm case.

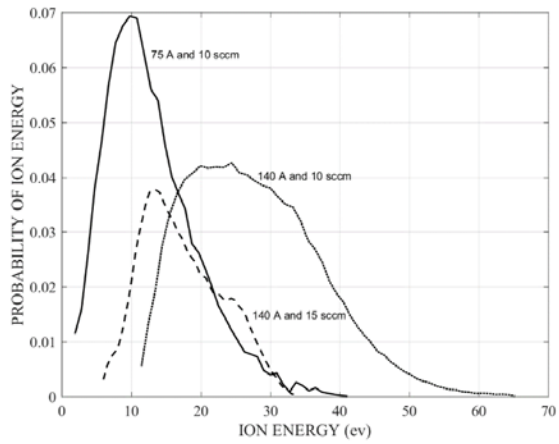

Figure 10. Ion energy distributions for the three operating conditions, taken with a RPA 10 cm off centerline.

Armed with these simplifications and local plasma measurements, we evaluate Eq. 1 to find the average erosion across the radial distance of the keeper face. We show Fig.11 the predicted erosion that would result after a 100 hour wear test. The error bars stem from uncertainty in the sputtering yield (see Appendix). This figure indicates a significantly high amount of erosion in the last operating condition compared to the erosion expected in the other two operating conditions. This demonstrates that provided the turbulent energy and ion content downstream of the keeper is in fact indicative of the processes at the keeper face, we can expect higher erosion at the HE case compared to the M1 and M2 cases. Moreover, it is evident that this predicted erosion should be greater than erosion that can be attributed to classical effects. The erosion due to classical mechanisms using the experimental discharge voltage as the ion energy, which is similar to the results generated by the OrCa2D code, if not underestimating the results. In conjunction with the calculated erosion, the expected classical erosion is generated using a first principals numerical code called the Orificed Cathode 2D (OrCa2D)[16]. The code takes in a number of free parameters including discharge voltage and emitter temperature to simulate plasma conditions inside the cathode and the plume of the cathode in order to calculate sputtering at the keeper face. It does not take into account anomalous ion heating. OrCa2D has recently been tailored to our cathode, and validated by experimental results.

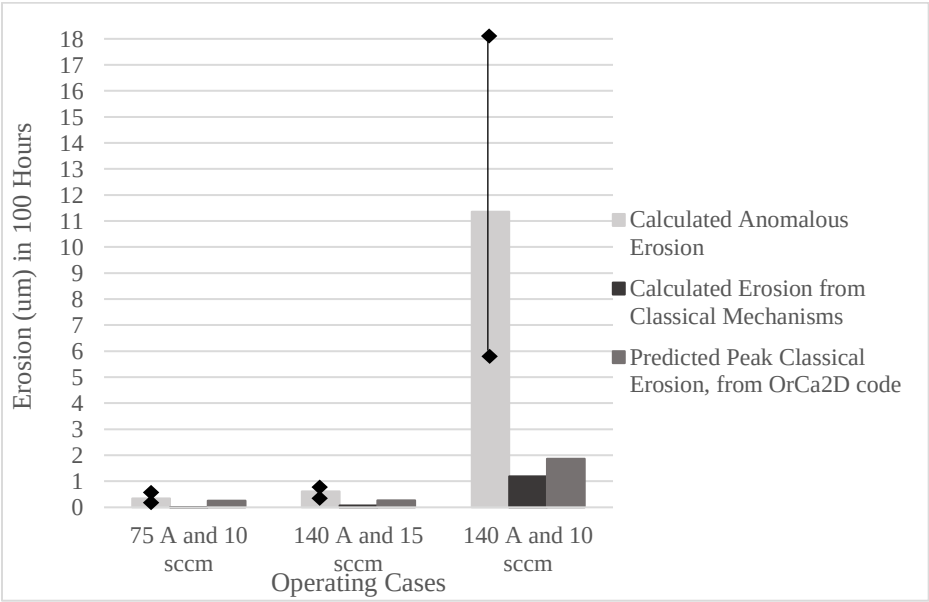

Figure 11. Plot comparing the average calculated erosion (from the RPA measurements) across the face of the molybdenum keeper in 100 hours with upper and lower bounds and the predicted peak classical erosion in 100 hours generated by the OrCa2D code, for each of the three operating conditions of interest.

When we compare the calculated erosion with the peak predicted classical erosion, there is a clear indication that the predicted high erosion is a result of anomalous processes. Armed with this predictive erosion, we conduct the experiment to verify if the erosion is mitigated based on this technique.

IV. Experimental Results

A. Mitigation Technique 1

As stated before, because of possible stress relief deforming the material during the first 25 hours, the keeper face after 25 hours became the new initial reference. As seen in the concentric plots in Fig. 12, the first wear test indicated very little erosion occurring at the edge of the cathode keeper orifice. The concentric plots indicated very little change between the 25 hour case and the 125 hour case.

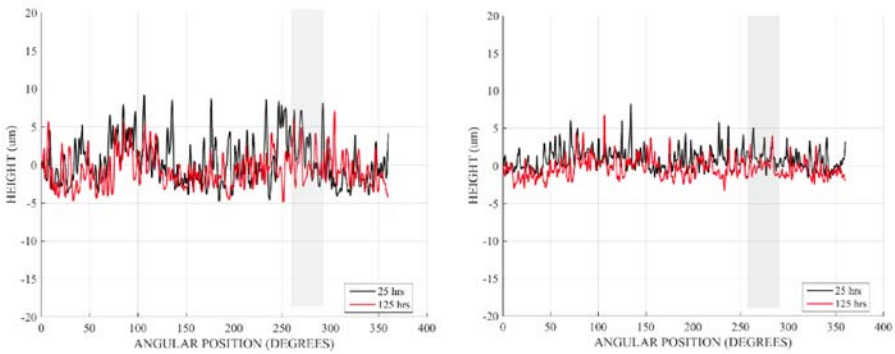

(a) (b)

Figure 12. Concentric profiles after running at 75 A and 10 sccm for 25 hours and 125 hours at a radial location a.) near the inner edge of the keeper orifice and b.) away from the inner orifice.

The overall average erosion (Fig. 13) indicates a small amount of erosion near the inner orifice of the keeper. The erosion is small enough and well within the noise of the data, that we can attribute the erosion to be due to classical mechanisms.

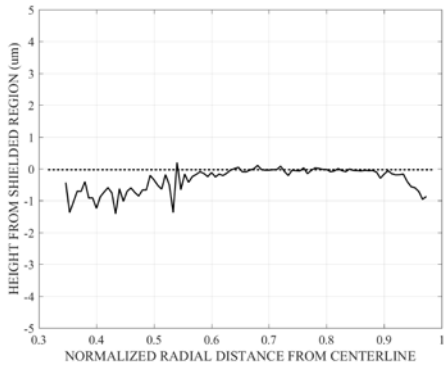

Figure 13. Average keeper erosion after 100 hours operating at 75 A and 10 sccm.

B. Mitigation Technique 2

The second wear test saw discernably more erosion occurring at the edge of the keeper orifice, as seen in Fig.14, with a peak erosion of around 3.5 um in 100 hours. One thing to note at this case was that the region of the keeper face away the orifice saw perhaps 1 mm of deposition from the tungsten liner in the anode in the 25 to 50 hour interval, as seen in Fig.15. This is seen in the average erosion across the keeper face, using the 25 hour as the initial reference. This possible deposition is certainly within the level of noise (as is the amount of erosion), and a comparison of the 50 hour keeper face to the 125 hour keeper face (Fig. 16 and 17) still indicates a similar average erosion rate. Fig. 18 shows the average erosion rate of the inner radius of the keeper, by fitting a best-fit line through the averaged erosion across 5% of the keeper radius, where the peak erosion occurs, for each subsequent 25 hour case. Omitting the 25 hour case still derives a very similar erosion rate, indicating that the erosion rate is linear.

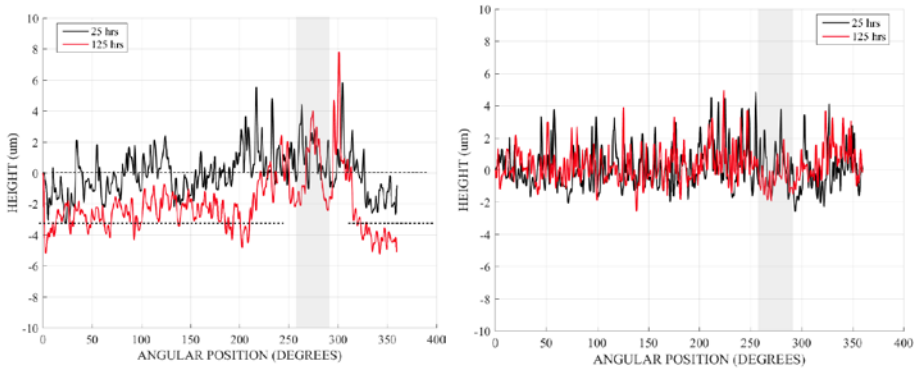

(a) (b)

Figure 14. Concentric profiles after running at 140 A and 15 sccm for 25 hours and 125 hours at a radial location a.) near the inner edge of the keeper orifice and b.) away from the inner orifice. The dotted line on the 125 hour profile represents the average value of the eroded surface, in reference to the zeroed shielded region.

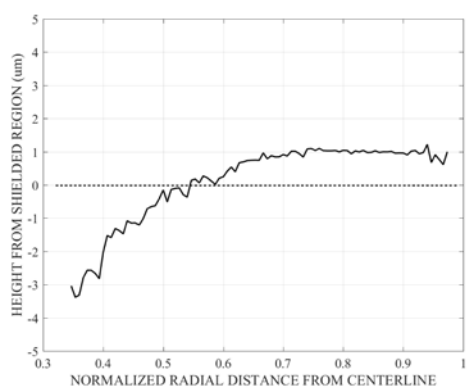

Figure 15. Average keeper erosion after 100 hours operating at 140 A and 15 sccm.

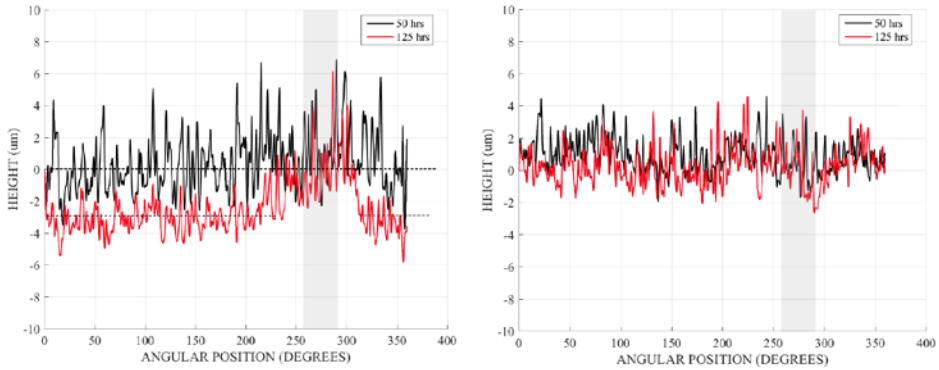

(a) (b)

Figure 16. Concentric profiles after running at 140 A and 15 sccm for 50 hours and 125 hours at a radial location a.) near the inner edge of the keeper orifice and b.) away from the inner orifice.

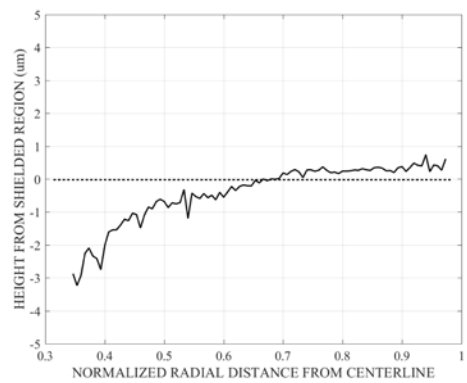

Figure 17. Average keeper erosion after 75 hours operating at 140 A and 15 sccm.

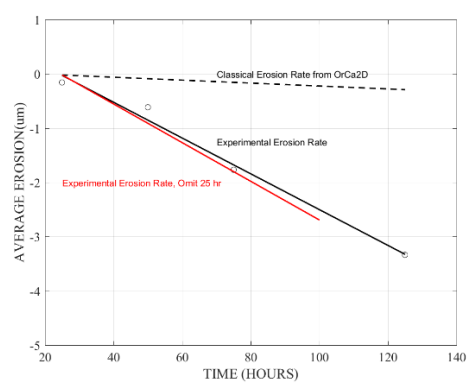

Figure 18. Average experimental erosion rate for the second mitigation case, taken as an average over 5% of the radial distance from the inner edge of the orifice (where peak erosion occurs); with the average 25 hour case included and without.

We must note that while the peak erosion (3.5 um) is within the noise of the raw data, this amount of erosion is higher than both the calculated anomalous erosion (1.1 um) and the predicated classical erosion (0.3 um) from the OrCa2D code, as shown in Fig. 18. As such, there is a possibility that not all of the anomalous high energy ions have

been killed off at this condition. But as seen in the subsequent condition, the peak erosion found at this case is significantly smaller than the peak erosion in the third operating condition.

C. High Erosion Condition

The third wear test was conducted twice because the tungsten liner failed during the first trial, perhaps due to an unstable plume mode. Uncompromised data was only collected up to the 75th hour, and then sometime during the last 50 hours the liner failed, causing deposition of copper onto the face of the keeper and obscured the erosion.

Prior to the second trial of the third wear test, the entire surface of the molybdenum keeper was polished down to remove the effects of the previous two wear tests. Unfortunately, the tungsten liner on the anode was misaligned during the 25 hour case, causing a new layer of copper deposition onto the face of the molybdenum keeper. Due to the ambiguity of the 25 hour trial results, the 25 hour case became the new initial reference.

(a) (b)

Figure 19. a.) Keeper face after polishing b.) Keeper face after 25 hours operating at 140 A and 10 sccm.

Because copper has a significantly higher sputtering rate than molybdenum[13], as demonstrated in Fig. 20, we can reasonably assume that whatever thin layer of copper deposited on the face of the keeper in those 25 hours would be sputtered off sometime during the rest of the wear test. In any case, polishing the surface of the keeper has allowed the shielded region to become an uncompromised reference to the eroded surface of the keeper in the next 100 hours.

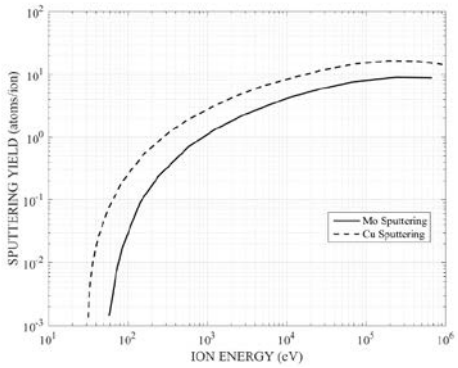

Figure 20. From Yamamura's plots of ion-induced sputtering yields from monatomic solids at normal incidence, the sputtering yield fit of Copper and Molybdenum from Xenon ion bombardment from experimental data[13].

Furthermore, the erosion rate observed during the first 75 hours is consistent with the erosion rate observed during the second trial, eliminating some measure of uncertainty (Fig. 24). The final wear test condition saw a significant amount of erosion occurring, as the entire keeper face was sputtered during both trials of the last operating condition instead of just at the inner edge of the orifice keeper (see Fig. 22). While the average erosion across the unshielded region of the keeper face was only slightly higher than the peak erosion occurring at the inner orifice in the previous cases, there were in fact places on the keeper face that saw twice the amount of erosion than that of the average. During the second trial, at places at the inner edge of the orifice, the keeper saw a peak erosion of 7 um in 100 hours, with an average 4 um of erosion across the entire keeper. During the first trial, the average erosion across the keeper was about 3 um in 75 hours with a peak erosion of 5 or 6 um (Fig. 21). This is very consistent with the amount of erosion observed in the second trial. When we compare this peak 7 um of erosion from the experiment to the peak 1 um of erosion expected from classical mechanisms, we can reasonably conclude the presence of high energy ions in this condition.

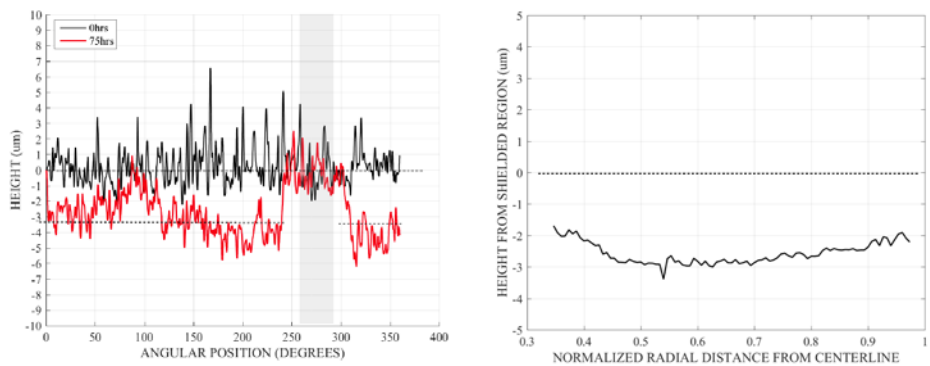

(a) (b)

Figure 21. a.) Comparison of an initial hour concentric profile with the 75 hour profile and b.) Average erosion across the face of the keeper after 75 hours for the first trial running the cathode at the high erosion condition.

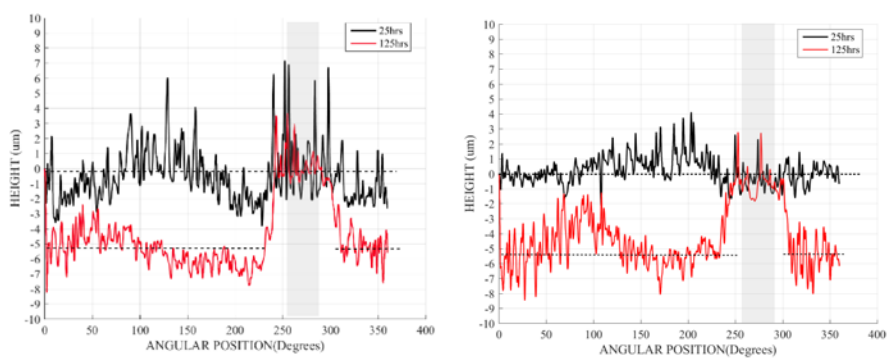

(a) (b)

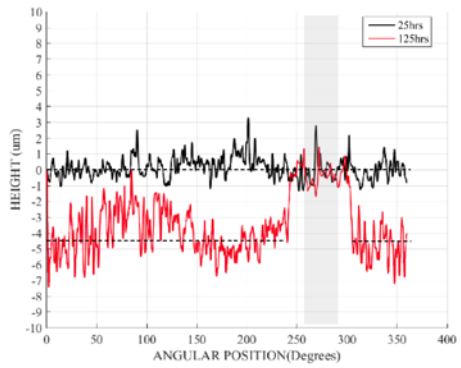

(c)

Figure 22. Concentric profiles after running at 140 A and 10 sccm for 25 hours and 125 hours at a radial location a.) near the inner edge of the keeper orifice and b.) and c.) away from the inner orifice.

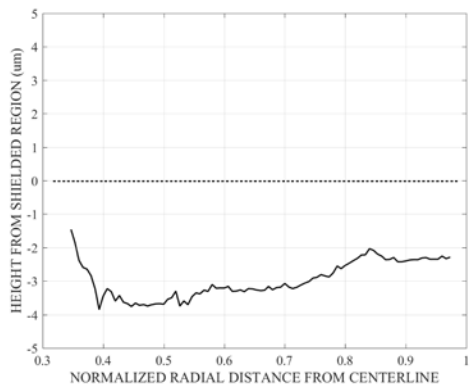

Figure 23. Average keeper erosion after 100 hours operating at 140 A and 10 sccm.

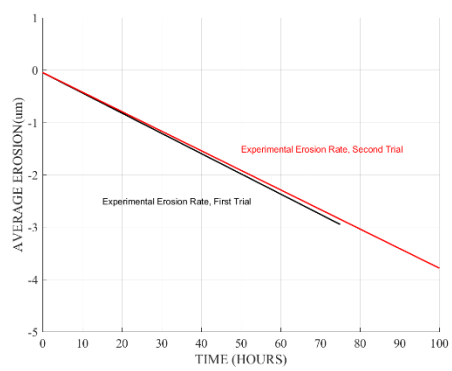

Figure 24. Average experimental erosion rate comparison for the first and second trials of the high erosion condition.

When we compare the peak erosions across each operating condition and compare them to the peak classical erosion expected, there is a significant difference between the two values at the theoretically high erosion operating condition (Fig.25). The error bars on the experimental results are driven by the noise on the raw data. The first operating conditions found a peak erosion that was comparable to the expected classical erosion generated by the OrCa2D code

and well within the data uncertainty of the raw scans. The second operating condition did find an experimental erosion higher than the calculated anomalous or classical erosion, which indicates that, although this higher erosion is within the noise of the raw data, the anomalous high energy ions may still exist at this condition. However, there is a very stark difference in erosion magnitude and pattern, when compared to the last operating condition. By decreasing the flow rate of xenon gas by 5 sccm, the peak erosion doubled in magnitude. Furthermore, as visually demonstrated in Fig. 26, the entire face of the keeper was sputtered during the last operating condition, as opposed to the just at the inner edge during the last two operating conditions.

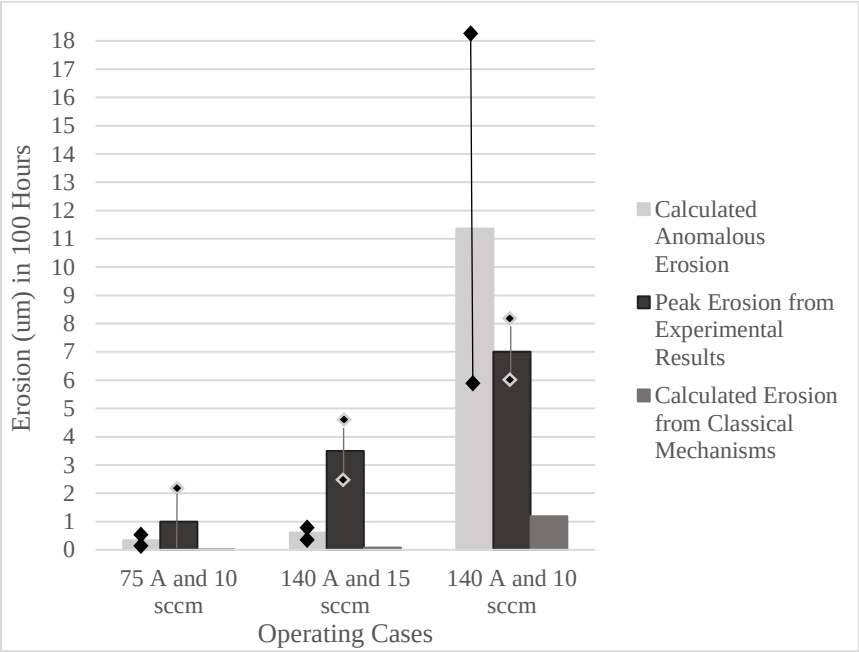

Figure 25. Plot of the calculated anomalous erosion from Sec. III, predicted peak classical erosion in 100 hours and the peak erosion obtained from the experimental results for each of the three operating conditions of interest.

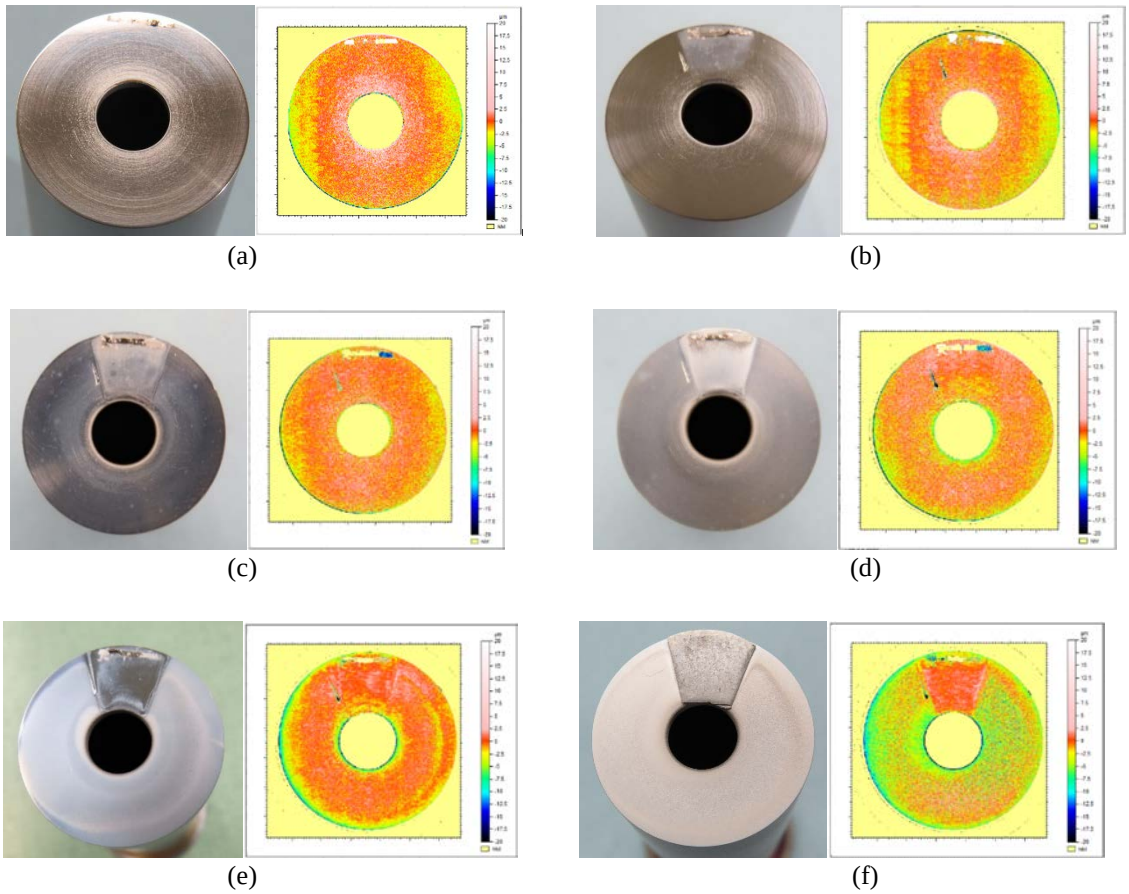

Figure 26. Photo and profilometer scan of keeper face for a.) reference hour (25 hrs) at first operating condition, b.) final hour (125 hrs) at first operating condition, c.) reference hour (25 hrs) at second operating condition, d.) final hour (125 hrs) at second operating condition, e.) reference hour (25 hrs) at third operating condition, and f.) final hour (125 hrs) at operating condition.

V. Conclusion

Previous studies have indicated IAT as a possible source of anomalous high energy ions and had identified operating conditions at which the presence of high energy ions would lead to theoretical high erosion on the face of the keeper. In this study, we have directly verified that the keeper face experiences anomalously high erosion at the indicated operating condition, especially in comparison to the two theoretically low erosion cases. The peak erosion that occurred at the 140 A and 10 sccm case was significantly higher than that predicted by classical mechanisms, by almost a factor of 7. Not only that, the entirety of the keeper face was sputtered at the last operating condition, as opposed to just at the edge of the orifice seen in the first two operating conditions. While experimental results indicate that possibly not all anomalous ions are quenched by this mitigation technique (as seen in the second operating condition), we have verified that a significant amount of erosion can be reduced by optimizing the operating conditions. The results of any future wear tests similar to the one conducted in this study would benefit from running the cathode for longer periods of time, to resolve erosion outside of the profilometer measurement noise. Still, the resulting verification of the erosion mitigation techniques outlined in this study has important implications in improving the lifespan of the high current cathodes called for in the next generation of EP missions.

Acknowledgment

The research described in this paper was carried out at the Jet Propulsion Laboratory, California Institute of Technology, under a contract with the National Aeronautics and Space Administration. The authors are indebted to Ray Swindlehurst and Nowell Niblett for their assistance throughout the research campaign. The authors also thank Jose Uribe for polishing the molybdenum keeper face.

APPENDIX

A general sputtering rate relation is given by Bohdansky[9] for monatomic solids at normal incidence:

$$\gamma(E) \sim \alpha s_n^{TF}(E)\left[1-\left(\frac{E_{th}}{E}\right)^{2/3}\right]\left[1-\frac{E_{th}}{E}\right]^2 \tag{3}$$

Where E is ion energy, E_{th} is threshold energy, α is an energy-independent function of the mass ratio between the target and projectile from Sigmund's original derivation[10], and s_n^{TF} is the Thomas-Fermi nuclear stopping cross section. A modification of the Bohdansky model in Eq. 3 was proposed by Garcia-Rosales[11], suggesting that for low ion energies, the Thomas-Fermi nuclear stopping cross section could be replaced with the Kr-C potential:

$$s_n^{KrC}(\epsilon) = \frac{0.5\ln(1+1.2288\epsilon)}{\epsilon + 0.1728\sqrt{\epsilon} + 0.008\epsilon^{0.1504}} \tag{4}$$

The reduced energy, ϵ, is

$$\epsilon = E\frac{M_2}{M_1 + M_2}\frac{a_L}{Z_1 Z_2 e^2} \tag{5}$$

Z_1 and Z_2 is the atomic numbers of the projectile (xenon) and target (molybdenum) particles, respectively, e^2 = 14.4 eV Angstrom, and a_L is the Lindhard screening length[11]:

$$a_L = 0.4685\left(Z_1^{2/3} + Z_2^{2/3}\right)^{-1/2} \tag{6}$$

Using the derived empirical formulas for sputtering yield by Eckstein[12] and Yamamura[13] as a guide, Sekerak et al.[14] selected a simplified empirical fit for the sputtering yield at low energies:

$$\gamma(E) = s_n^{KrC}(\epsilon)e^{\beta-\left(\frac{E-V_k}{E_{th}}\right)^{\eta}} \tag{7}$$

Where V_k is the keeper voltage and β, η, and E_{th} are fit parameters derived by Sekerak et al.[14] from a curve fit of literature values by Doerner for molybdenum sputter yield from xenon ion bombardment at normal incidence angle. The sputtering yield fit to Doerner data[15] is recreated below for convenience:

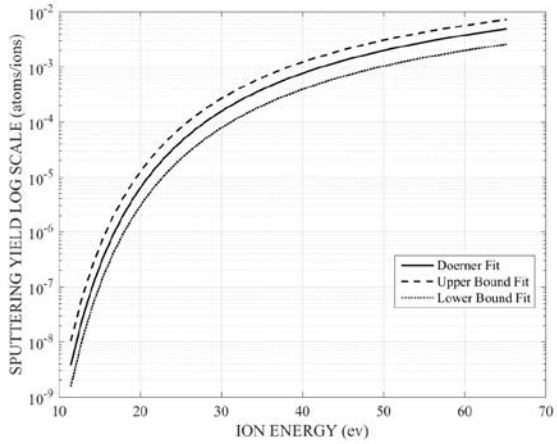

Figure 27. Replotted fit with upper and lower bounds by Sekerak[14] to the data provided by Doerner[15] for molybdenum sputtering yield from xenon ion bombardment.

Fit Parameter	Doerner Fit	Upper Bound	Lower Bond
E_{th} (eV)	120	115	122
η	1.15	1.15	1.15
β	1.0	1.3	0.4

Table 1. Molybdenum sputtering fit parameters provided by Sekerak for Eq. 7, with upper and lower bounds.

References

[1]Jorns, B. A., Goebel, D. M., and Mikellides, I. G., "Investigation of Energetic Ions in a 100-A Hollow Cathode," 50th AIAA/ASME/SAE/ASEE Joint Propulsion Conference, Cleveland, OH, July 28-30, 2014. AIAA-2014-3826.

[2]Jorns, B. A., Mikellides, I. G., Lopez-Ortega, A. and Goebel, D. M., "Mitigation of energetic ions and keeper erosion in a high-current hollow cathode," 34th International Electric Propulsion Conference, Kobe, Japan, July 4-10, 2015. IEPC-2015-134.

[3]Friedly, V. and Wilbur, P., "High current cathode hollow cathode phenomena," *Journal of Propulsion and Power,* Vol. 8, No. 3, 2008, pp. 635-643.

[4]Mikellides, I. G., Katz, I., Goebel, D.M., and Polk, J. E., "Hollow cathode theory and experiment II: A two-dimensional theoretical model of the emitter region," *Journal of Applied Physics,* Vol. 98, No. 11, 2005, pp. 113303.

[5]Mikellides, I.G., Katz, I., Goebel, D.M., and Jameson, K., "Evidence of nonclassical plasma transport in hollow cathodes of electric propulsion." *Journal of Applied Physics,* Vol. 101, No. 6., 2007, pp. 063301.

[6]Jorns, B. A., Mikellides, I.G., Goebel, D.M., "Temporal Fluctuations in a 100-A LaB6 Hollow Cathode", 33rd International Electric Propulsion Conference, Washington D.C., Oct 6-10, 2013. IEPC-2013-385.

[7]Bychenkov, V., Silin, V., and Uryupin, S., "Ion-acoustic turbulence and anomalous transport," *Physics Reports,* Vol. 164, No. 3, 1988, pp. 119-215.

[8]Sagdeev, R., and Galeev, A., *Nonlinear plasma theory,* Frontiners in physics, W. A. Benjamin, 1969.

[9]Bohdansky, J., "A universal relation for the sputtering yield of monatomic solids at normal ion incidence," *Nuclear Instruments and Methods in Physics Research Section B: Beam Interactions with Materials and Atoms,* Vol 2., No. 1-3, March 1984, pp. 587-591.

[10]Sigmund, P., “Theory of Sputtering. I. Sputtering Yield of Amorphous and Polycrystalline Targets,” *Physical Review*, Vol. 184, No. 2, Aug 1969, pp. 383-416.

[11]Garcia-Rosales, C., Eckstein, W., and Roth, J., “Revised formulae for sputtering yield,” *Journal of Nuclear Materials*, Vol. 218, No.1, Jan. 1995, pp.8-17.

[12]Eckstein, W. and Preuss, R., “New fit formulae for the sputtering yield,” *Journal of Nuclear Materials*, Vol. 320, No. 3, Aug. 2003, pp. 209-213.

[13]Yamamura, Y., and Tawara, H., “Energy Dependence of Ion-Induced Sputtering Yields from Monatomic Solids at Normal Incidence,” *Atomic Data and Nuclear Data Tables*, Vol. 62, No. 2, March 1996, pp. 149-253.

[14]Sekerak, M.J., Hofer, R.H., Polk, J.E., Jorns, B.A., Mikellides, I.G., “Wear Testing of a Magnetically Shielded Hall Thruster at 2000 s Specific Impulse”, 30th International Symposium on Space Technology and Science, 34th International Electric Propulsion Conference, Hyogo-Kobe, Japan, July 6-10, 2015. IEPC-2015-155/ISTS 2015-b-155.

[15]Doerner, R.P., Whyte, D.G., and Goebel, D.M., “Sputtering yield measurements during low energy xenon plasma bombardment”, *Journal of Applied Physics*, Vol. 93, No. 9, 2003. Pp. 5816.

[16]Ortega-Lopez, A., Mikellides, I.G., and Jorns, B.A., “First-principles Modeling of IAT-driven Anomalous Resistivity in Hollow Cathode Discharges II: Numerical Simulations and Comparisons with Experiments”, 35th International Electric Propulsion Conference, Salt Lake City, Utah, 2016.

[17]J. R. Brophy and C. E. Garner, “Tests of High Current Hollow Cathodes for Ion Engines,” AIAA-88-2913, 24th AIAA/ASME/SAE/ASEE Joint Propulsion Conference, Boston, Massachusetts, July 11–13, 1988.

[18]Polk, J., Anderson., Brophy, J., Rawlin, V., Patterson, M., Sovey, J., and Hamley, J., “An overview of the results from an 8200 hour wear test of the NSTAR ion thruster,” 35th AIAA/ASME/SAE/ASEE Joint Propulsion Conference, June 20-24,1999, Los Angeles, CA. AIAA-99-2446.

[19]Sengupta, A., Brophy, J.R., and Goodfellow, K.D., “Status of the extended life test of the Deep Space 1 flight spare ion engine after 30,352 hours of operation,” 39th AIAA/ASME/SAE/ASEE Joint Propulsion Conference, July 20-23, 2003, Huntsville, AL. AIAA-03-4558.

[20]Williams, G., Smith, T., Domonkos, M., Gallimore, A., and Drake, R., “Laser-induced uorescence characterization of ions emitted from hollow cathodes," Plasma Science, IEEE Transactions on, Vol. 28, No. 5, 2000, pp. 1664-1675.

[21]Williams, G., Domonkos, M. T., and Chavez, J. M., “Measurement of doubly charged ions in ion thruster plumes," 27th International Electric Propulsion Conference, Oct. 14-19, 2001. Pasadena, CA. IEPC-01-310.

[22]Foster, J. E. and Patterson, M. J., “Downstream Ion Energy Distributions in a Hollow Cathode Ring Cusp Discharge," Journal of Propulsion and Power, Vol. 21, No. 1, Jan. 2005, pp. 144-151.

[23]Goebel, D. M., Jameson, K. K., Katz, I., and Mikellides, I. G., “Potential fluctuations and energetic ion production in hollow cathode discharges," Physics of Plasmas, Vol. 14, No. 10, 2007.

[24]Chu, E., Goebel, D. M., and Wirz, R. E., “Reduction of Energetic Ion Production in Hollow Cathodes by External Gas Injection," Journal of Propulsion and Power, Vol. 29, No. 5, June 2013, pp. 1155-1163.

[25]Latham, P., Pearce, A., and Bond, R., “Erosion processes in the UK-25 ion thruster," 22nd International Electric Propulsion Conference, Oct, 1991, Viareggio, Italy, IEPC-91-096.

[26]Kameyama, I., “Effects of Neutral Density on Energetic Ions Produced Near High-Current Hollow Cathodes," Tech. Rep. NASA CR-204154, Oct. 1997.

[27]Katz, I., Mikellides, I. G., Goebel, D. M., Jameson, K. K., and Johnson, L., “Production of high energy ions near an ion thruster discharge hollow cathode," 42nd AIAA/ASME/SAE/ASEE Joint Propulsion Conference and Exhibit, July 9-12, 2006. Sacramento, CA. AIAA-2006-4485.

[28]Gallimore, A. and Rovey, J., “Erosion Processes of the Discharge Cathode Assembly of Ring-Cusp Gridded Ion Thrusters," Journal of Propulsion and Power, Vol. 23, No. 6, 2007, pp. 1271-1278.

[29]Mikellides, I. G., Katz, I., Goebel, D. M., Jameson, K., and Polk, J., “Wear Mechanisms in Electron Sources for Ion Propulsion, II: Discharge Hollow Cathode," Journal of Propulsion and Power, Vol. 24, No. 4, 2008, pp. 866-879.

[30]Mikellides, I. G., Goebel, D. M., Jorns, B. A., Polk, J., and Guerrero, P., “Numerical Simulation of the Partially-ionized Gas in a 100-A LaB6 Hollow Cathode," 33rd International Electric Propulsion Conference, October 6 - 10, 2013, Washington, D.C. IEPC-2007-124.

[31]Dodson, C., Perez-Grande, D., Jorns, B. A., Goebel, D. M., and Wirz, R. E., "Laser-induced Fluorescence Measurements of Energetic Ions in a 100-A LaB6 Hollow Cathode", 52nd AIAA/SAE/ASEE Joint Propulsion Conference, Salt Lake City, Utah, 2016.